The 8th International Supercritical CO_2 Power Cycles Symposium
February 27 – 29, 2024, San Antonio, Texas
Paper #4

Increasing Main Cooler Thermal Performance for sCO_2 Power Cycles

Matthew Searle*[,1,2]
Research Scientist

Doug Straub[1]
Research Engineer

[1] National Energy Technology Laboratory, 3610 Collins Ferry Road, Morgantown, WV 26505, USA
[2] NETL Support Contractor, 3610 Collins Ferry Road, Morgantown, WV 26505, USA

Dr. Matthew Searle works as a NETL Support Contractor at the National Energy Technology Laboratory (NETL). Matthew received his PhD in Mechanical Engineering from Brigham Young University in 2018. Matthew's area of expertise is experimental thermal science. Research areas of interest include turbine blade aerothermal design, heat transfer in sCO_2 power cycles, and enhanced heat transfer through advanced manufacturing.

Doug Straub is a Research Engineer at the U.S. Department of Energy's National Energy Technology Laboratory and has over 30 years of experience in the fields of experimental combustion and heat transfer. Doug's publications and patents have been widely cited and cover a diverse range of topic areas. Doug has been instrumental in developing several unique experimental capabilities at NETL, including the high-pressure CO_2 flow loop to measure average heat transfer coefficients and pressure drop at 200 bar.

ABSTRACT

Increasing sCO_2 power cycle cooler performance will increase the efficiency and lower the cost of electricity for sCO2 power cycles. This work considered the heat transfer performance of two counter-flow, shell-and-tube heat exchangers using local measurements. The heat exchangers were constructed using commercial tubing. One heat exchanger was constructed with a conventional, smooth inner tube (7 mm nominal inner diameter). The other was constructed with an additively manufactured tube with a square cross section and angled rib turbulators. For mixed mean temperatures away from the pseudocritical temperature, the heat transfer coefficient matched the Dittus-Boelter correlation. As the mixed mean temperature approached the pseudocritical temperature, the heat transfer coefficient deviated from the Dittus-Boelter correlation due to transverse property variation and buoyancy. The local and average heat

*Corresponding author: matthew.searle@netl.doe.gov

transfer coefficients for angled rib tubes were nominally 150% to 300% greater than the heat transfer coefficients for the smooth tube. Trends in heat exchanger effectiveness indicated that the ribs were most beneficial when the water flow rates were at the low end of the range considered: 0.016 – 0.126 kg/s. Using results from prior system modeling, it is anticipated that adding heat transfer enhancement features in a cycle cooler will increase the sCO_2 cycle efficiency by 0.34 percentage points.

INTRODUCTION

Motivation

Supercritical carbon dioxide (sCO_2) power cycles have the potential to transform the U.S. power generation sector through power generation solutions with higher efficiency, smaller footprints, and increased heat source flexibility than existing systems (Brun et al., 2017).

The recuperated Brayton cycle is of interest for both direct (oxy-fuel combustion) and indirect (fossil, concentrated solar, and nuclear) cycles. The cost and performance of the heat exchangers in the recuperated Brayton cycle are major factors in plant cost and cycle efficiency (Brun et al., 2017).

Previous research has focused on improving the performance of the high and low temperature recuperators (indirect and direct) as well as the primary heater (indirect) with efforts to increase the specific (mass-weighted) effectiveness of these heat exchangers (Searle, 2020; Robey, 2022). It is anticipated that heat exchanger cost may be reduced significantly by increasing specific effectiveness through enhanced convective heat transfer rather than increased surface area.

More recently, system studies have identified that improving the effectiveness of the cycle main cooler can significantly improve system performance. One study showed that the cycle efficiency increases by 2-4 percentage points and the cost of electricity (COE) decreases by 3-8% as the cooler outlet temperature decreases by 10-15 °C (Pidaparti et al., 2020).

Literature Review

The state-of-the-art heat exchanger technology for sCO_2 power cycles (including main coolers) is the printed-circuit-heat-exchanger (PCHE) (Jiang et al., 2018a). This heat exchanger consists of diffusion-bonded layers with chemically etched channels. An additional technology which has proven more difficult to use in practice is the micro-shell-and-tube heat exchanger. However, it is competitive from a thermal performance standpoint (Jiang et al., 2018b). One avenue to fabricate a more robust micro-shell-and-tube heat exchanger is through additively manufacturing the entire structure as a single part.

The present study of heat transfer enhancement in cooler tubes is part of a larger effort to make additively manufactured heat exchangers cost competitive with existing PCHE technology.

The NETL Heat Exchange and Experimental Test (HEET) facility has previously reported on the thermo-fluid performance of smooth and enhanced tubes for sCO_2 cycle recuperators and internal cooling features for direct-cycle turbine cooling. These studies employed the Wilson plot technique to report heat transfer performance (Black et al., 2020; Roy et al., 2022; Searle et al., 2020).

The present study demonstrates, as expected, that for sCO_2 flow in a cooler, the property variations are sufficiently large that local measurements are required to determine the heat transfer performance.

It is well known that in the vicinity of the pseudocritical line that the thermophysical properties vary dramatically. Further, heat transfer coefficients become large. The enhancement is due in part to the property variations, but it has also been demonstrated that buoyancy and flow acceleration effects resulting from the property variation can enhance or degrade the heat transfer (Jackson, 2017).

The contributions of the present study are two-fold: first, compare experimental data to existing correlations and, second, consider the heat transfer performance enhancement realized by using angled rib features on the sCO_2 side in an additively manufactured architecture.

Materials and Methods

The materials and methods of this study are now discussed. First, the test article design and instrumentation are introduced. Next, the test conditions are listed. The experimental approach, which employs local temperature measurements, and differs from prior Wilson plot efforts, is described. Finally, the uncertainty analysis is discussed.

Test Articles

Two counter-flow, shell-and-tube test heat exchangers were fabricated using commercial tubing and fittings. In one test article, the center tube was conventional, commercial tubing. In the second, it was an additively manufactured tube with a square inner cross-section and angled rectangular ribs on two sides. A schematic of the overall setup is displayed in Figure 1.

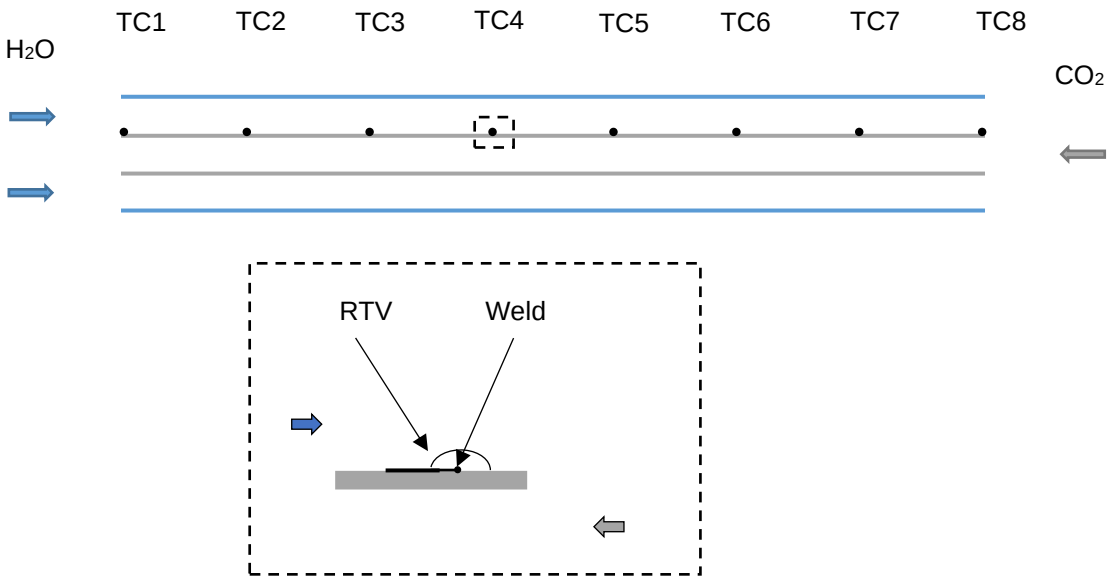

Figure 1: Test article layout.

In Figure 2, a drawing and picture of the ribs is displayed. Water flowed through the shell tube and CO_2 flows through the inner tube. Thermocouples (TC) with 0.8 mm diameter sheaths were routed through the shell wall using a commercial compression fitting and affixed at 13 cm intervals along the tube outer wall with tack welds. As shown in the inset, after each thermocouple was welded to the tube outer wall, it was protected with a small bead of room-temperature-vulcanizing (RTV) silicone. Test article parameters are shown in Table 1.

Test conditions were selected to be representative of the working fluid temperature, pressure, and Reynolds number of a main cooler and are reported in Table 2.

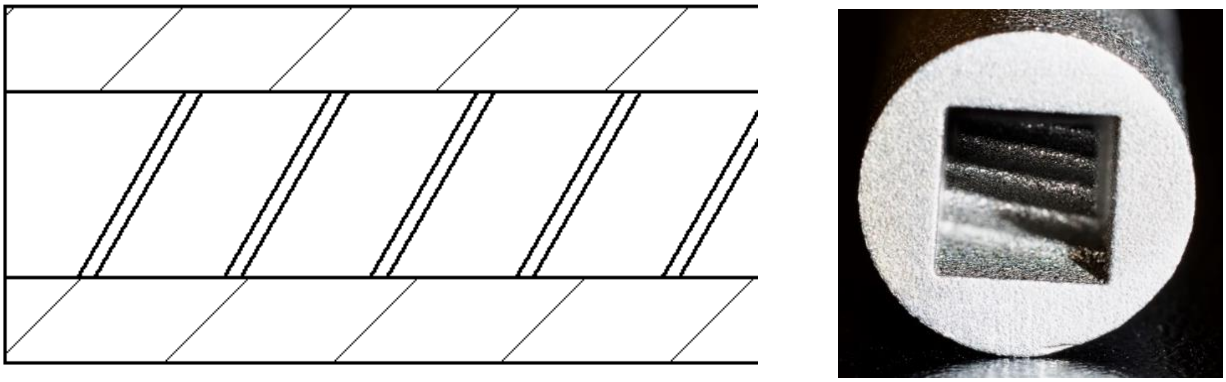

Figure 2: Schematic and picture of rib-featured tube considered in present effort.

Table 1: Test article parameters.

Parameter	Symbol	Value
Heat Exchanger Length	L	1.04 m
Inner Hydraulic Diameter	D_h	4.98 mm
Outer Hydraulic Diameter	$D_{h,o}$	4.7 mm
Rib Height	e	0.39 mm
Rib Pitch	P	3.91 mm
Rib Depth		0.39 mm
Rib Angle	α	60°
Rib Pitch to Height	P/e	10
Rib Height to Hydraulic Diameter	e/D_h	0.078

Table 2: Test parameters table.

CO_2 (Tube)		
Inlet Temperature (K)	$T_{t,i}$	349.8
Inlet Pressure (MPa)	$P_{t,i}$	8
Mass Flow Range (kg/s)	$\dot{m}_t$	0.0089 to 0.015
Reynolds Number Range, (-)	Re_t	8×10^4 *to* 1.3×10^5
Water (Shell)		
Inlet Temperature (K)	$T_{s,i}$	289
Inlet Pressure (MPa)	$P_{s,i}$	0.136
Mass Flow Range (kg/s)	$\dot{m}_s$	0.016 – 0.126

Experimental Approach

The experimental approach is now introduced. First, details concerning the facility operation are provided, then the data reduction procedure is described, and a computational fluid dynamics (CFD) simulation is employed to verify the data reduction approach.

To achieve the operating temperature and pressure, the CO_2 working fluid was circulated while heat was applied, and CO_2 was injected using a syringe pump. The water flow rate and CO_2 mass flow rate were adjusted to test conditions. Once a steady state was reached and verified by achieving a standard deviation on the tube side pressure transducer less than 10 Pa, data was recorded for five minutes while the system was stable at the condition.

The data, acquired every five seconds, was averaged over the five-minute intervals and results for inlet and outlet fluid temperature, gauge and differential pressure, mass flow, and local wall temperature measurements were acquired.

The experimental approach assumed a uniform axial heat flux distribution to reduce the data. To develop confidence in this approach, a CFD simulation was performed. In Figure 3, results of the CFD analysis and data reduction procedure using the CFD data as input are shown. In panel (a), q'' is shown vs. location. Results for the CFD calculation are shown with orange markers and the simulated experiment results are shown with blue markers. As expected, a uniform heat flux is observed for the simulated experiment. The trend in heat flux for the CFD results is concave up and shows greater deviation from the simulated heat flux at the CO_2 inlet than the outlet.

The heat transfer coefficient is shown vs. location in panel (b) for both the CFD data and the simulated experiment. Here it is shown that the maximum deviation for the simulated experiment from the CFD calculation is 15%. As expected, h increases with decreasing location, primarily driven by the large variation in properties near the pseudocritical line.

Detailed results for the CFD simulations will be reported in a future paper. A summary of the CFD conditions is reported here. The simulation conditions match the experiment sCO_2 inlet temperature and pressure, 350 K and 8 MPa. The sCO_2 Reynolds number is 1×10^5 and the coolant water flow is 0.05 kg/s. A commercial CFD software was utilized to mesh and solve the simulation domain. The simulation domain consisted of the water flow in the shell, the sCO_2 flow in the tube, and the tube wall separating the flows. REFPROP property values for the sCO_2 flow were entered at 50 points spanning the realizable temperature range. Uniform properties for the water were assumed at the inlet temperature (288 K) and pressure (0.101 MPa). The properties of the 316 stainless-steel tubes were assumed to be uniform and were taken from material property data.

Turbulence was modeled using the shear stress transport (SST) k-ω turbulence model with enhanced wall treatment. Cell size was selected to be 0.5 mm after a mesh refinement study indicated that decreasing the mesh size to 0.4 mm only changed the average Nusselt number on the tube side by 1.6%. Inflation layers were applied at the shell and tube walls with the maximum number of layers being 20 and the growth rate being 1.2.

The pressure-velocity coupled solver with the energy equation enabled was iterated using a pseudo-transient mechanism until the variation in the parameters of interest (heat transfer coefficient, wall temperature) were less than 1% and the simulation residuals decreased below 1×10^{-6}.

Having demonstrated that the uniform heat flux assumption is valid, the experimental data reduction procedure is now discussed. The uniform heat flux was calculated using an energy balance across the tube flow volume. Thermophysical properties were calculated in the Python data reduction script with CoolProp and benchmarked against thermophysical properties calculated in Excel with REFPROP 10. To determine temperature variation in the sCO_2 through the heat exchanger, the tube flow volume was discretized into segments corresponding to the local thermocouple locations. Energy balances were performed across these discretized elements to determine the local temperature.

The local heat transfer coefficient was calculated at discrete points using Newton's Law of cooling.

$$q" = h(T_w - T_m)$$

where $q"$ is the wall heat flux, T_w is the measured wall temperature, and T_m is the mixed mean temperature obtained from q" and the discretized energy balance.

The conductive resistance of the tube wall relative to the convective resistance at the water and CO_2 wall interfaces is negligible. Further, conjugate heat transfer within the tube is small. Thus, the heat transfer coefficient may be calculated using wall temperature measurements without additional error other than that arising from the individual thermocouple accuracy.

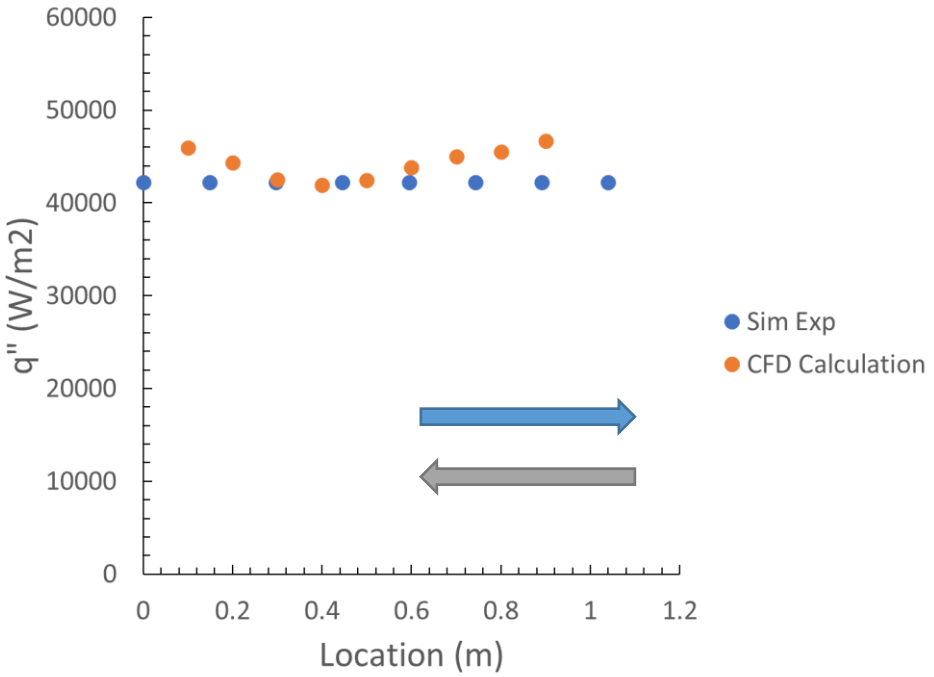

Panel (a)

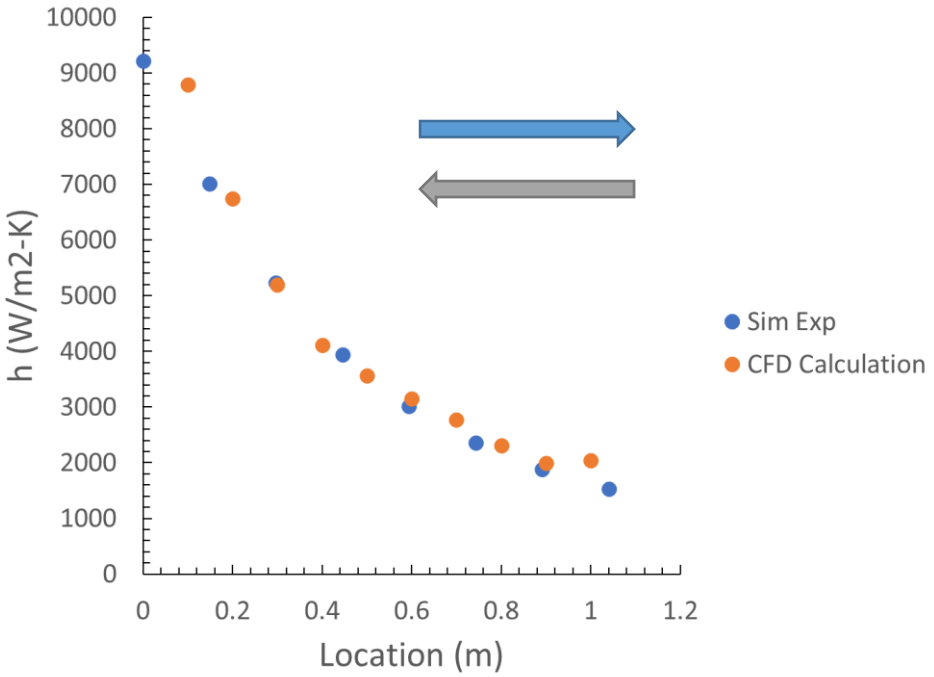

Panel (b)

Figure 3: Panel (a) heat flux, q'', vs. location for simulated experimental data points and CFD calculation. Panel (b) heat transfer coefficient vs. location. The simulation conditions match the experiment temperature and pressure. The sCO_2 Reynolds number is 1×10^5 and the coolant water flow is 0.05 kg/s.

Uncertainty Analysis

Uncertainty in the reported experimental values was calculated using the Kline and McClintock approach (Kline & McClintock, 1953). Details of instrument uncertainties and uncertainty analysis for the HEET test facility have been reported previously (Searle, 2020). This study adds local thermocouple measurements and the uncertainty in these were ±2 K. Error bars for the overall uncertainties are reported in the figures and the errors were calculated using the same approach.

RESULTS AND DISCUSSION

The results of this study are now discussed. First, local wall temperature and heat transfer coefficient trends are introduced. Next, the trend in the surface area averaged heat transfer coefficient, $\bar{h}$, with the heat flux to mass flux ratio, Q''/G, is discussed. The local results are compared to correlations to assess their utility. Finally, the overall performance of the lab-scale heat exchanger is scaled and implications for cycle heat exchanger performance are discussed.

Temperature Plots

The non-dimensional wall temperature θ_w is defined.

$$\theta_w = (T_w - T_{s,i})/(T_{t,i} - T_{s,i})$$

$\theta_w = 0$ indicates that the wall temperature equals the inlet water temperature, $T_{s,i}$. $\theta_w = 1$ indicates that the wall temperature equals the CO_2 inlet temperature, $T_{t,i}$.

Plots of θ_w vs. x are shown in Figure 4. In panel (a), results are shown for flow through conventional tubes. In panel (b), results are shown for flow through square tubes with angled rib features. For both panels, θ_w decreases as the water flow rate increases. As expected, θ_w decreases as x decreases indicating that the wall cools as the flow is cooling. An important observation is that a 30% increase in θ_w occurs at x > 0.6 m in the angled rib tube relative to the conventional rib tube.

Local Heat Transfer Coefficient

Results for the local heat transfer coefficient are now introduced. In Figure 5, plots of h vs. x are displayed at three water mass flow rates spanning 0.016 kg/s to 0.063 kg/s. Results for the conventional tube and the tube with the angled ribs are shown in panels (a) and (b), respectively. It is noted that the fifth thermocouple for the conventional tube failed prior to tests and thus a temperature measurement is absent near x = 0.6 m. Several points are important to make concerning these plots. First, the heat transfer coefficient, h, increases as the sCO_2 cools towards the pseudocritical temperature, 307.8 K. Second, h increases as the water flow rate increases. This is attributed to increased convection due to flow buoyancy. Finally, comparing panel (a) and (b), h is higher for the angled ribs than the smooth conventional tube. This effect is attributed to enhanced heat transfer resulting from the flow separation, re-attachment, and turbulence introduced by the angled ribs.

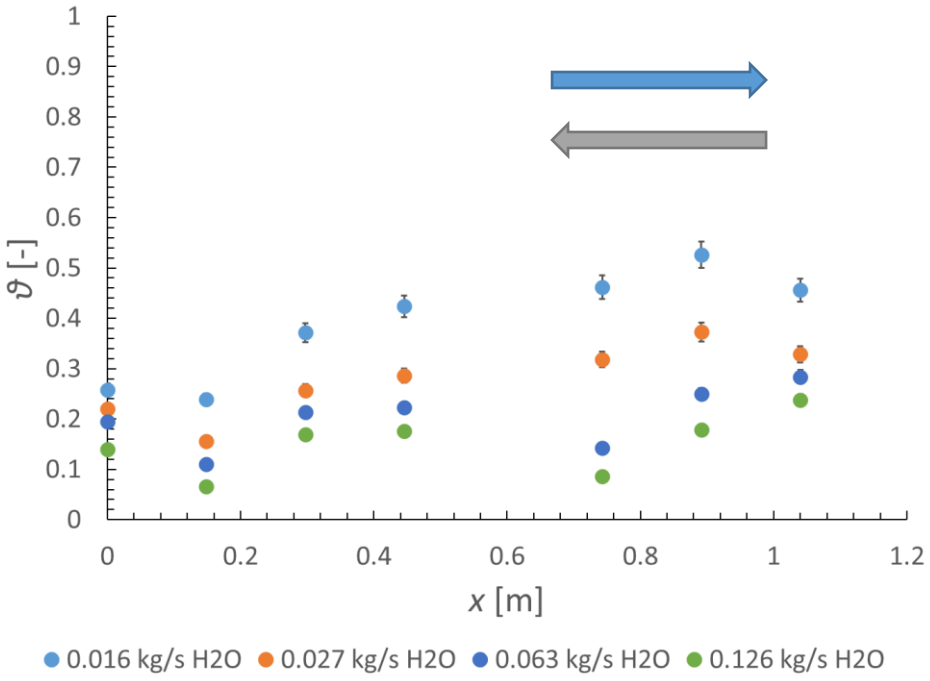

Panel (a)

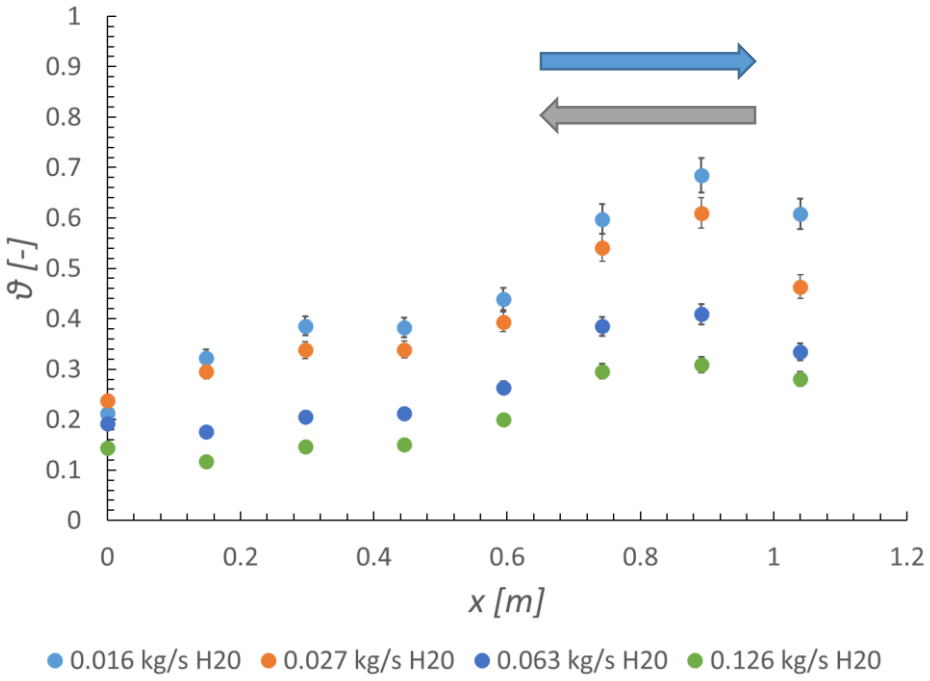

Panel (b)

Figure 4: Panel (a) Plot of θ_w vs. axial location x for water flow rates 0.016 kg/s to 0.126 kg/s in heat exchanger with conventional tube. Panel (b) Plot of θ_w vs. axial location x in additively manufactured tube square cross section tube with rib turbulators. CO_2 (gray) and water (blue) flow directions are indicated on chart with arrows.

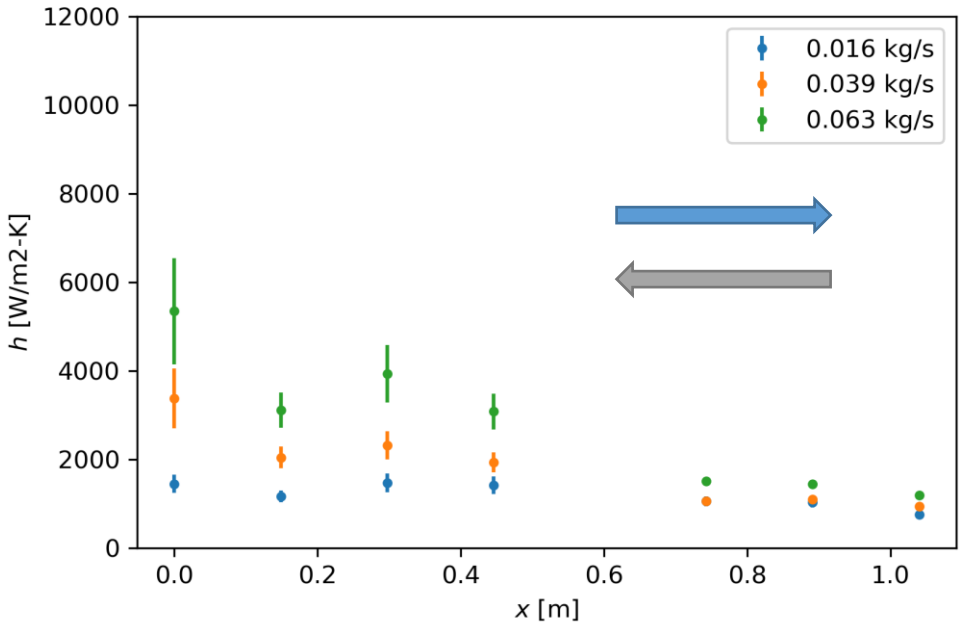

Panel (a)

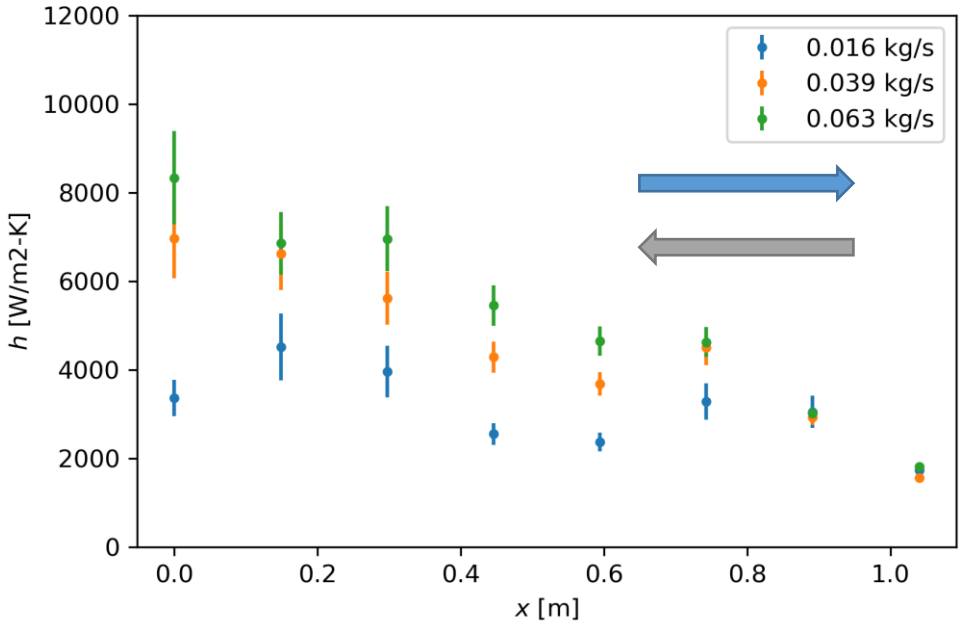

Panel (b)

Figure 5: Local heat transfer coefficient, h, as a function of axial position, x. CO_2 (gray) and water (blue) flow directions are indicated on chart with arrows. Water flow rates are at 0.016 kg/s, 0.039 kg/s, and 0.063 kg/s.

In Figure 6, the local heat transfer coefficient, h, is plotted vs. the local bulk temperature scaled by the pseudocritical temperature, T/T_{pc}. It is important to note that all data were acquired for a tube Reynolds number of $Re = 1 \times 10^5$. In panel (a), results for the smooth conventional tube are shown and are compared to the Dittus-Boelter and Yoon correlations (Yoon, 2003). In panel (b), results for square tube with additively manufactured rib elements are shown. Here, predictions for the Dittus-Boelter correlation and a correlation for angled rib turbulators (Han and Park, 1988) are displayed. The Yoon correlation was selected at the recommendation of a review of pseudocritical CO2 heat transfer correlations (Ramesh, 2021) and the Han correlation at the recommendation of a review of gas turbine cooling correlations (Sundberg, 2006).

In general, the heat transfer coefficient increases as T/T_{pc} approaches 1. This is due to fluid property variations near the pseudocritical line. Further, this trend is apparent regardless of whether heat transfer enhancement features are present in the tube.

The Yoon correlation is consistently higher than the Dittus-Boelter correlation. This is due to property variation transverse to the fluid flow and buoyancy-induced secondary flow. Typical Richardson numbers, Ri, for the flow are two orders of magnitude higher than the criterion for buoyancy, $Ri = 10^{-3}$ (Pidaparti, 2019). The Dittus-Boelter correlation is within the uncertainty of the experimental data at $T/T_{pc} > 1.08$. For $T/T_{pc} < 1.08$, , h increases more quickly than the value predicted by the Dittus-Boelter correlation. For T/T_{pc} < 1.04, the Yoon correlation is within the uncertainty interval of the experiments and the Dittus-Boelter correlation is well below the lower uncertainty bound. This match to the Yoon correlation at values of T close to T_{pc} is attributed to greater transverse property variation and stronger buoyancy in the flow.

The heat transfer data in panel (b) for the additively manufactured tube with ribs is now compared to the correlation. For $T/T_{pc} > 1.02$, the Han and Park 1988 correlation is well below the lower uncertainty bound for the experimental data. There are two contributing factors that act together to cause this effect. First, the additively manufactured tube exhibits intrinsic surface roughness that enhances the heat transfer beyond that observed in the channels with smooth surface features considered in Han's experiment. Second, the Han correlation was developed only for airflow past rib turbulators. In that scenario, transverse property variation is small and buoyancy is not present.

Average Heat Transfer Coefficient Results

In Figure 7, $\bar{h}$ is plotted vs. $Q"/G$ for both conventional tubing and angled ribs. The tube inlet Reynolds number is 1×10^5. For the experimental results, the surface area averaged heat transfer coefficient, $\bar{h}$, increases as the surface heat flux to mass flux ratio increases. The Dittus-Boelter correlation calculated at the flow inlet Reynolds number and Prandtl number is shown. The value predicted by Dittus-Boelter is constant since effects of transverse property variation and buoyancy were not accounted in the correlation development. However, it is helpful to note that the correlation falls within the uncertainty interval of the data at $Q"/G = 80$, and that is in agreement with the local heat transfer coefficient measurements As the position in the tube at which the mixed mean temperature reaches the pseudocritical temperature moves up the tube from the tube outlet toward the tube inlet, the average heat transfer coefficient increases, due to property variation and buoyancy.

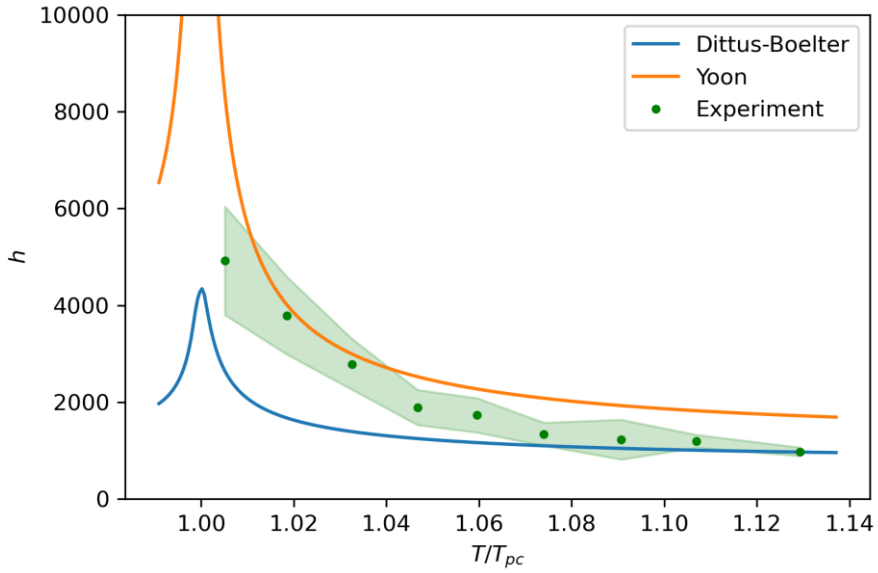

Panel (a)

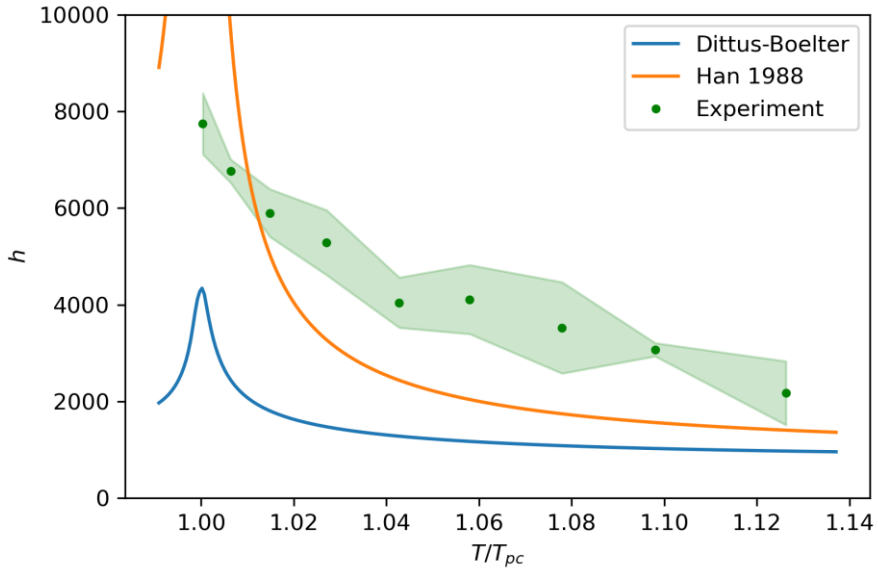

Panel (b)

Figure 6: Local heat transfer coefficient, h, vs. T/T_{pc}. Results for conventional (Panel a) and angled rib tubes (Panel b). Predictions by the Dittus-Boelter, Yoon (2003), and Han and Park (1988) correlations are displayed for comparison.

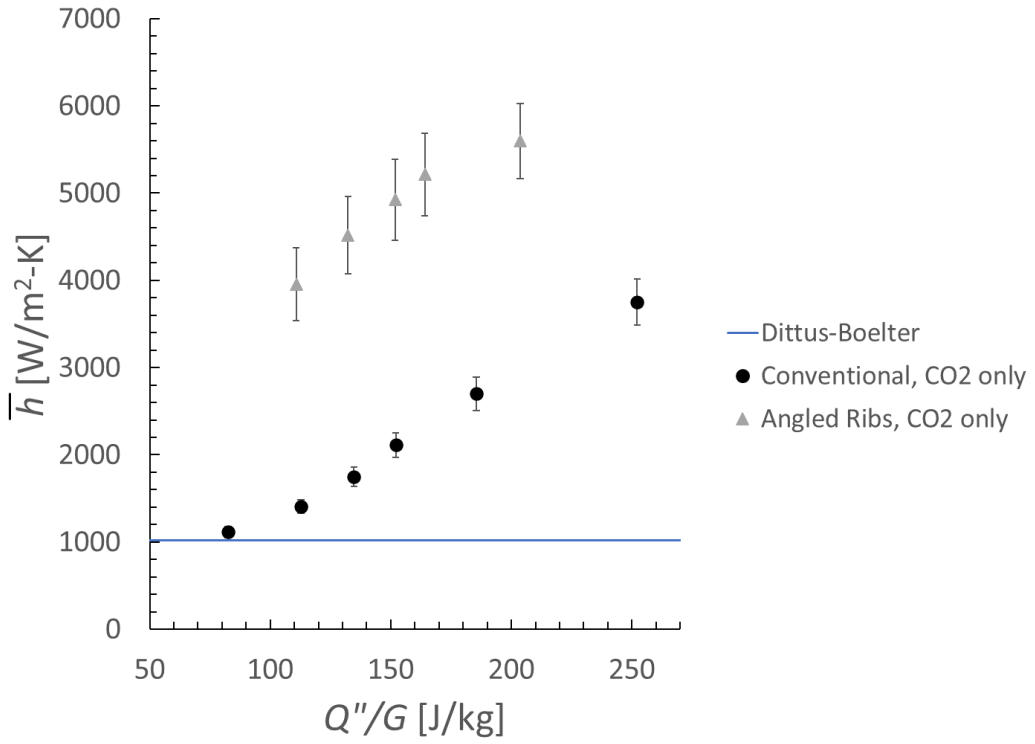

Figure 7: $\bar{h}$ vs. Q"/G. Results displayed for conventional tubing and angled ribs. Dittus-Boelter correlation calculated for tube inlet conditions.

As expected from the local heat transfer results, the average heat transfer coefficient for the rib patterned tube is 150 to 300 percent greater due to the enhanced heat transfer arising from the boundary layer separation and reattachment and enhanced turbulence arising due to the presence of the ribs.

Pressure drop and friction factor results

In Figure 8, friction factor, f, is shown as a function of $Q"/G$ for both angled rib tubes and conventional tubes.

Friction factor is independent of $Q"/G$ for the conventional tube and shows a slight downward trend for the angled ribs. The cause of the downward trend in angled ribs is due to the larger change in fluid properties across the test section due to the higher cooling rate.

Overall Performance of Lab-scale Heat Exchanger

To describe the overall performance of the heat exchanger, the heat exchanger effectiveness, ε, is calculated.

$$\varepsilon = (T_{t,i} - T_{t,o})/(T_{t,i} - T_{s,i})$$

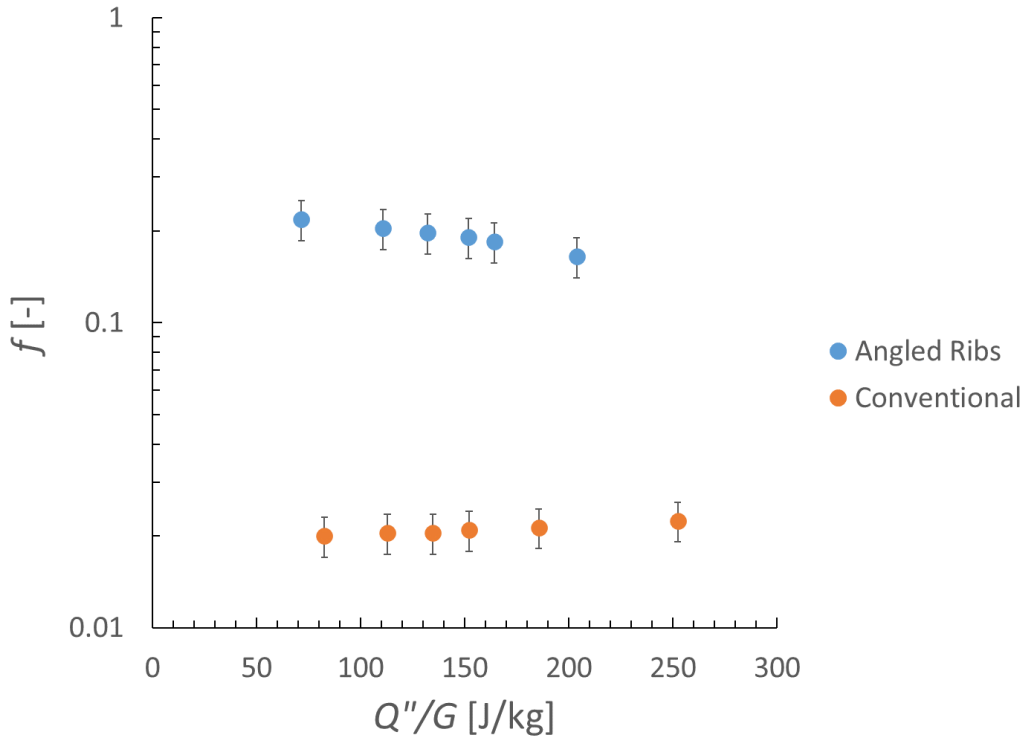

Figure 8: f vs. Q"/G for angled rib tubes and conventional tubes.

Results are plotted for this performance factor vs. the shell (water) flow rate in Figure 9. Data for both angled rib tubes and conventional tubes are shown at two tube-side Reynolds numbers, Re_t: 9×10^4 and 1.3×10^5.

A prior study considered main cooler performance for sCO_2 cycles (Pidaparti, 2020). Several cooler configurations were considered: wet evaporative, water-based indirect, and direct, dry cooling. In Figure 10, cycle efficiency (%) for the wet evaporative cooling are plotted vs. heat exchanger effectiveness. As a first observation, the test shell-in-tube heat exchanger is not optimized, since the ε values span 0.4 to 0.7 (experiments, Figure 9) while the cycle ε values span 0.65 to 0.92 (system model, Figure 10). However, the trends in Figure 9 are expected to be similar for the cycle heat exchangers. It is observed that the introduction of angled rib tubes increases ε on average by 13% (a 0.072 increment) over the range of water flows considered at $Re_t = 1.3 \times 10^5$. If even half the effectiveness increment (0.036) were achieved in a plant heat exchanger with ε = 0.65, the expected net plant efficiency gain would be 0.34 percentage points.

While increasing cooler effectiveness at specific inlet conditions, could improve power cycle performance and possibly improve market penetration. A second approach to increase market penetration of sCO2 power cycles, would be to design a cooler at fixed effectiveness (corresponding to optimized power cycle system studies (Pidaparti, 2020)) and utilize heat transfer enhancement techniques to reduce the volume of material necessary to build the heat exchanger. For many heat exchanger applications, heat exchanger cost decreases as the material quantity and heat exchanger volume decrease. This is particularly true for the serial deposition process utilized in additive manufacture.

It is important to emphasize that a lower cost, additively manufactured heat exchanger cannot currently be achieved by replacing conventional heat exchanger components with heat transfer enhanced additively manufactured components alone since the cost of additively manufactured copies of conventional parts can be one to two orders of magnitude more expensive than the conventional parts themselves. The cost reduction would result by eliminating the assembly and joining process and accompanying specialty tooling required to assemble and manifold heat exchangers. A future technoeconomic study could leverage the results of this paper to assess if the observed performance improvements would significantly reduce cost.

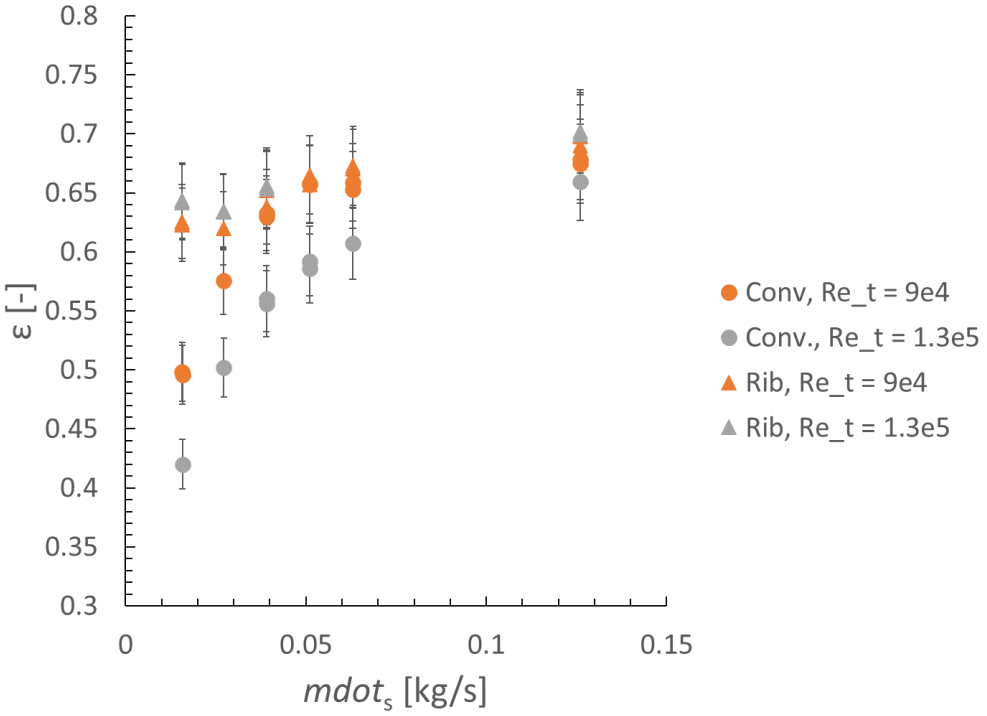

Figure 9: Heat exchanger effectiveness, ε, as a function of cooling water flow rate for both conventional tube and angled rib featured tubes. The tube side Reynolds number, Re_t, equals 9×10^4 and 1.3×10^5.

CONCLUSIONS

The thermal performance of a lab-scale sCO_2 cooler was determined. Local wall temperature measurements were made to determine the local heat transfer coefficient and hydraulic performance was characterized by pressure drop measurements. The following conclusions were drawn from this effort.

- The experimental heat transfer coefficient data for the smooth, conventional tube agreed within experimental uncertainty with the Dittus-Boelter correlation for $T/T_{pc} > 1.08$. At $T/T_{pc} < 1.08$, the heat transfer coefficient for the conventional tube was greater than the Dittus-Boelter correlation and agreed with the Yoon correlation for $1.01 < \frac{T}{T_{pc}} < 1.04$ within experimental uncertainty.

- The local and average heat transfer coefficient for angled rib tubes were nominally 150% to 300% greater than the smooth tube. Further, heat transfer enhancement decreased modestly as T/T_{pc} decreased to 1.

- The increase in heat exchanger effectiveness due to the angled rib tubes was greater at low water flow rates and high sCO_2 Reynolds numbers.

- A 13% increase in heat exchanger effectiveness (0.072 increment) was typical for the rib patterned cooler considered in this study. If even half the effectiveness increment (0.031) could be achieved for a plant cooler, the cycle efficiency gain would be 0.34 percentage points.

Future work could identify optimum enhancement features for cycle coolers and explore integrating heat transfer enhancement features in a monolithic, additively manufactured heat exchanger. Further, additional cycle modeling could verify the predicted efficiency gains.

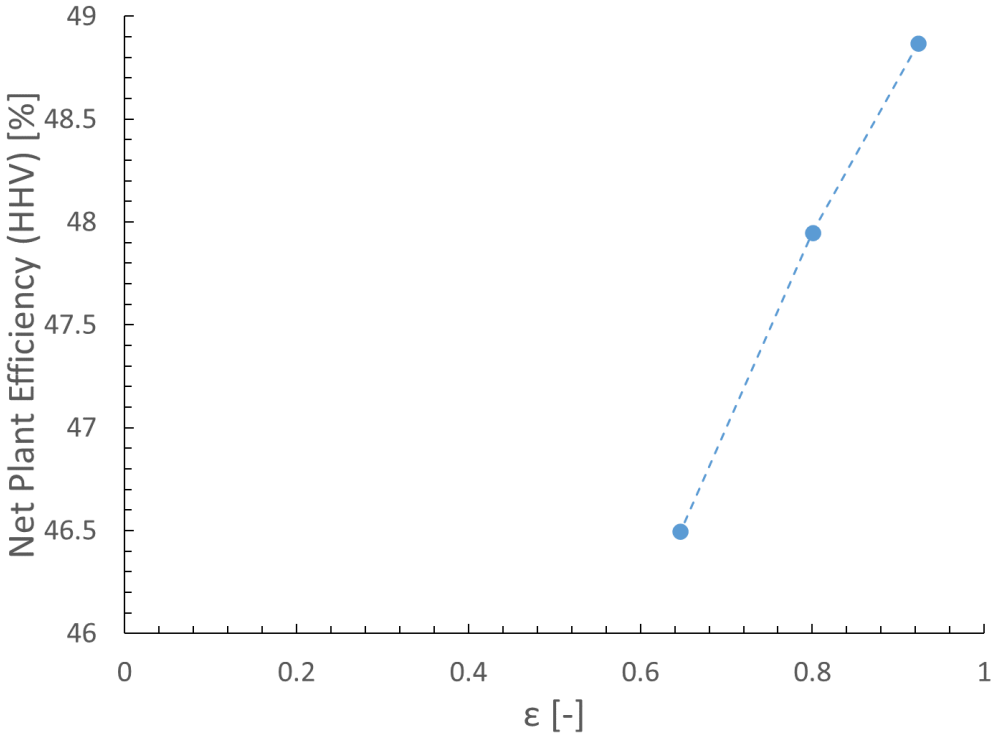

Figure 10: Prior system model predictions for net plant efficiency (HHV) vs. ε for plant with wet evaporative coolers (White, 2020; Pidaparti, 2020; Ahmed, 2023).

REFERENCES

Black, J., Straub, D., Robey, E., Yip, J., Ramesh, S., Roy, A., & Searle, M. (2020). Measurement of Convective Heat Transfer Coefficients with Supercritical CO2 Using the Wilson-Plot Technique. Journal of Energy Resources Technology, 142(7). https://doi.org/10.1115/1.4046700

Brun, K., Friedman, P., & Dennis, R. (2017). Fundamentals and Applications of Supercritical Carbon Dioxide (sCO2) Based Power Cycles. Woodhead Publishing.

Han, J. C. and Park, J. S. (1988). Developing Heat Transfer in Rectangular Channels with Rib Turbulators, *International Journal of Heat and Mass Transfer*, 31, 183-195.

Jackson, J. D. (2017). Models of heat transfer to fluids at supercritical pressure with influences of buoyancy and acceleration. Applied Thermal Engineering, 124, 1481–1491. https://doi.org/10.1016/j.applthermaleng.2017.03.146

Jiang, Y., Liese, E., Zitney, S. E., & Bhattacharyya, D. (2018a). Design and dynamic modeling of printed circuit heat exchangers for supercritical carbon dioxide Brayton power cycles. Applied Energy, 231, 1019–1032.

Jiang, Y., Liese, E., Zitney, S. E., & Bhattacharyya, D. (2018b). Optimal design of microtube recuperators for an indirect supercritical carbon dioxide recompression closed Brayton cycle. Applied Energy, 216(January), 634–648. https://doi.org/10.1016/j.apenergy.2018.02.082

Kline, S., & McClintock, F. (1953). Describing uncertainties in single-sample experiments. In Mechanical engineering.

Pidaparti, S. R. (2019). *Heat Transfer and Fluid Flow Characteristics of Supercritical Carbon Dioxide Flow,* Georgia Institute of Technology, Dissertation.

Pidaparti, S. R., White, C. W., & Weiland, N. T. (2020). Cooling System Cost and Performance Models to Minimize Cost of Electricity of Direct SCO2 Power Plants. The 7th International Supercritical CO2 Power Cycles Symposium, 1–22.

Ramesh, S. and D. Straub (2021). Review and Analysis of Heat Transfer Correlations for Horizontal Psuedocritical CO2 Heat Exchanger Applications. National Energy Technology Laboratory: Morgantown, WV.

Robey, E. H., Ramesh, S., Sabau, A. S., Abdoli, A., Black, J. B., Straub, D. L., & Yip, M. J. (2022). Design Optimization of an Additively Manufactured Prototype Recuperator for Supercritical CO2 Power Cycles. *Energy*, *251*, 12. https://doi.org/https://doi.org/10.1016/j.energy.2022.123961

Roy, A., Searle, M., Ramesh, S., & Straub, D. (2022). Investigation of Gas Turbine Internal Cooling using Supercritical CO2 – Effect of surface roughness and channel aspect ratio. Journal of Engineering for Gas Turbines and Power, 144(November 2022), 1–15. https://doi.org/10.1115/1.4055497

Searle, M., Black, J., Straub, D., Robey, E., Yip, J., Ramesh, S., Roy, A., Sabau, A. S., & Mollot, D. (2020). Heat transfer coefficients of additively manufactured tubes with internal pin fins for supercritical carbon dioxide cycle recuperators. Applied Thermal Engineering, 181(August), 116030.

Sundberg, J. (2006). Heat Transfer Correlations for Gas Turbine Cooling, Department of Mechanical Engineering, Linkoping University, Thesis.

Yoon, S. H., Kim, J. H., Hwang, Y. W., Kim, M. S., Min, K., and Kim, Y. (2003). Heat Transfer and Pressure Drop Characteristics during the In-Tube Cooling Process of Carbon Dioxide in the Supercritical Region, *International Journal of Refrigeration,* 26(8), pp. 857-864.

DISCLAIMER

ACKNOWLEDGEMENTS

This work was performed in support of the U.S. Department of Energy's Fossil Energy and Carbon Management's Turbines Research Program and executed through the National Energy Technology Laboratory (NETL) Research & Innovation Center's sCO_2 Field Work Proposal. The authors would like to acknowledge the contribution and expertise of site operations support contract personnel including Mr. Dennis Lynch, Mr. Rich Eddy, and Mr. Jeff Riley.